ADVANCED MATERIALS
www.advmat.de

Thermoplastic Molding of Chitosan to Form Living Plastic Materials

*Reddhy Mahle, Peggy Cebe, Nilotpal Majumder, Onur Hasturk, Glenn Leung, Chunmei Li, Weiguo Hu, Edward B. Gordon, Sanjana Gopalakrishnan, Yushu Wang, Sourabh Ghosh, and David L Kaplan**

Numerous approaches for the solution-based fabrication of chitosan-based materials are reported, but most often result in materials with limitations in terms of stability in aqueous systems and mechanics unless chemical cross-linking is utilized. In the present study, a thermomechanical compression method is presented for solid-state processing of chitosan powders into dense bulk plastic-like materials where the mechanical and physical properties can be tailored. To achieve this outcome, chitosan-citrate complexes, formed through ionic cross-linking and amidation, undergo thermal fusion at high temperature and pressure to generate robust materials with retention of the inherent properties of chitosan, including biodegradability and cytocompatibility. The chitosan-based plastics can be doped with enzymes and antibiotics with retention of bioactivity and are also explored as living materials when microbial cells (e.g., *Pseudomonas putida*) are included in the process and subsequently shown to maintain metabolic functions to degrade organic pollutants. This thermoplastic approach for solid-state processing of chitosan enables the development of a variety of new materials and composites with embedded biomolecules for enhanced functions. This solid-state fabrication of chitosan bulk materials approach eliminates the need for conventional solution-based processing, enabling rapid material production via compression molding while reducing costs, minimizing waste, and improving overall manufacturing efficiency.

1. Introduction

Biopolymers are invigorating worldwide research toward functional and responsive sustainable materials due to their biodegradability, recyclability, and biogenic point of origin.[1] Among proteins, polysaccharides, lipids, and polynucleotides, the polysaccharides constitute the most abundant portion of biomass and are therefore available in large quantities.[2] Chitosan, derived through partial or full deacetylation of chitin, is a polysaccharide with distinct arrangements of D-glucosamine and N-acetyl-glucosamine units.[2–4] The abundance of hydroxyl and amino groups in chitosan leads to intra and intermolecular hydrogen bonding resulting in an intricately woven molecular and hierarchical structures.[5,6] The unique molecular structure of chitosan exhibits exceptional physiochemical properties including solubility, viscosity, and biodegradability, tuned by external environmental factors such as pH and temperature, toward applications in biomedical materials,[7] tissue engineering,[8] drug delivery,[5] food and agriculture,[6] and bioelectronics,[9] among others.

Chitin is present in nature (e.g., crustacea, insects, fungi) as an insoluble polymer which often limits its applications, thus, requiring changes in chemistry (e.g., deacetylation) to modify functionally into chitosan.[10] Some fungi generate chitosan directly, but this is the exception as a direct green synthesis of chitosan from several Zygomycetes fungi such as *Absidia*, *Rhizopus*, and *Gongronella* where *G. butleri* has been reported for the highest direct yields of chitosan.[11] Chitosan is also approved by the US Food and Drug Administration (FDA) for its use as a biomaterial[12] and is considered as Generally Recognized As Safe (GRAS)[13] which provides utility for a wide range of applications. With the expanding potential of chitosan applications across diverse fields, recent research has focused on tailoring chitosan and its derivatives into various material formats, including nanofibers, microspheres, nanoparticles, hydrogels, membranes, and 3D-printed scaffolds.[3] Among these, chitosan membranes and films are particularly promising due to their versatility in fabrication methods and adaptability for

R. Mahle, O. Hasturk, G. Leung, C. Li, E. B. Gordon, S. Gopalakrishnan, Y. Wang, D. L Kaplan
Department of Biomedical Engineering
Tufts University
Medford, MA 02155, USA
E-mail: david.kaplan@tufts.edu

P. Cebe
Department of Physics and Astronomy
Tufts University
Medford, MA 02155, USA

N. Majumder, S. Ghosh
Department of Textile and Fibre Engineering
Indian Institute of Technology Delhi
New Delhi 110016, India

W. Hu
Conte Polymer Research Center
University of Massachusetts
Amherst, MA 01003, USA

The ORCID identification number(s) for the author(s) of this article can be found under https://doi.org/10.1002/adma.202511623

DOI: 10.1002/adma.202511623

applications such as food packaging, separation membranes, pollutant remediation, medical devices, and more.[14] Typically, chitosan films are produced by incorporating cross-linkers and plasticizers to enhance solubility, increase chain mobility, and improve mechanical properties.[15] Commonly used techniques, such as casting or solvent evaporation, involve treating chitosan with ionic liquids, glutaraldehyde, or acetic acid. However, these approaches often suffer from drawbacks including long processing times and the use of toxic solvents, which limit their environmental compatibility and biomedical applicability.[3,16] To address these limitations, recent efforts have pivoted toward employing biodegradable and biocompatible cross-linkers and plasticizers such as citric acid, choline chloride, glycerol, and genipin that enable the fabrication of chitosan films using methods like thermal pressing.[15,17] This not only reduces processing time but also results in environmentally friendly and safer chitosan materials.

In this work, we present a new approach to generate chitosan-based materials which offers an opportunity to design and fabricate customized dense, plastic-like material structures with stable shapes and excellent robustness. The process involves compacting polymeric glucosamine chains under controlled pressure and temperature in the presence of citric acid, which simultaneously acts as both a cross-linker and plasticizer. The key advantage of this thermomechanical technique lies in its tunable processing conditions, which allow control over the biochemical and mechanical properties of the resulting materials. The resulting dense, plastic-like chitosan structures exhibit versatility. Importantly, the relatively mild processing conditions support the integration of bioactive molecules such as enzymes and antibiotics into the chitosan matrix during fabrication. This enables the stabilization and retention of bioactivity without requiring covalent cross-linkers, which are traditionally used for immobilizing enzymes and microbes in the chitosan materials.[3,18] The tunability of processing conditions and the retention of bioactivity enabled the fabrication of chitosan-based bacterial plastics as living materials. *Pseudomonas putida*, a bacterium capable of degrading organic pollutants,[19] was utilized to generate self-supporting chitosan-based bulk living materials that exhibited phenol remediation activity.

2. Results and Discussion

2.1. Preparation of Chitosan Plastics

Chitosan is a linear poly-aminosaccharide obtained by alkaline deacetylation of chitin. The polymer is present in the exoskeletons of insects and crustaceans, and is found in lower eukaryotic organisms such as fungal cell walls, **Figure 1a**.[20] The abundance of hydroxyl and amino groups in the chitosan chains leads to intra and intermolecular hydrogen bonding, therefore limiting the solubility of chitosan in water and most organic solvents, Figure 1b.[21] The transformation of chitosan powder into chitosan-based dense plastic-like materials involved the plasticization of chitosan using citric acid, Figure 1c. Citric acid, being a triprotic acid with three pKa values: 3.13, 4.76, and 6.40, was used to solubilize chitosan by reducing the pH to ≈3 which is below the pK_a of the chitosan amino groups, therefore leading to protonated amine groups.[22] Chitosan, as a weak base, acts as a cationic polyelectrolyte with positively charged amino groups forming salt complexes with the negatively charged carboxylic groups in citric acid.[23] Subsequently, the complex that forms was stirred overnight at 80 °C leading to possible cross-linking between citric acid and chitosan.[24] The solution was a mix of electrostatically and covalently cross-linked chitosan and citric acid which is referred as Cs-CA solution. The excess citric acid was removed via dialysis of the Cs-CA solution against DI water until no residual citric acid was detected by mass spectrometry (Figure S1, Supporting Information). During dialysis, the pH increased to 5.1 leading to zeta potential dropping to 18 mV starting from 50 mV, due to reduced charge density (Table S1, Supporting Information). The removal of unbound citric acid and consequent deprotonation due to increasing pH causes intra- and inter-chain interactions in chitosan resulting in the formation of aggregates with citric acid cross-linked between the chains (Figures S2 and S3, Supporting Information).

The aggregate formation results in a water insoluble gel-like suspension which is lyophilized to prepare the Cs-CA powder. For the preparation of dense plastics, the Cs-CA powder is packed into predesigned molds and thermomechanically compressed at 632 MPa to be densified into bulk chitosan plastics. As a control, the chitosan powder as provided by the supplier, was also processed under similar pressure and temperature conditions. **Figure 2a–f** presents the photographs of the starting material, and the plastics obtained in the process which are prepared by thermomechanically compressing chitosan and Cs-CA powder at 632 MPa but at different temperatures, i.e., 60, 90, and 125 °C for 20 min to compare the outcomes.

The density of the chitosan plastic prepared at 125 °C in the form of discs was calculated to be 1.27 g cm^{-3} while the thermomechanically compressed pure chitosan powder yielded only a loosely compacted plastic. Scanning electron microscopy (SEM) images of the Cs-CA lyophilized powder showed flaky elongated forms(Figure 2g,h), which were previously observed for freeze-dried cross-linked chitosan hydrogels.[25,26] The chitosan plastics changed features with increased temperature during the thermomechanical compression process to densify the materials; the plastics prepared at higher temperature exhibited homogenous surface features and transparency. The cross-section electron microscopy images showed the bulk chitosan plastics prepared at 60 °C contained cracks and loosely compacted sides (Figure 2i), in comparison to the plastics prepared at the higher temperatures (90 and 125 °C). The plastics fabricated at these higher temperatures had more homogenous features (Figure 2j,k). The plastics also exhibited a visual transition from white to pale yellow to brown with increasing temperature from 60 to 125 °C. These changes in the chitosan plastics can be attributed to the molecular changes which were assessed using spectroscopic methods, described in the next section.

2.2. Material Characterization

The plasticization/cross-linking of chitosan using citric acid was studied and confirmed by spectroscopic and thermal

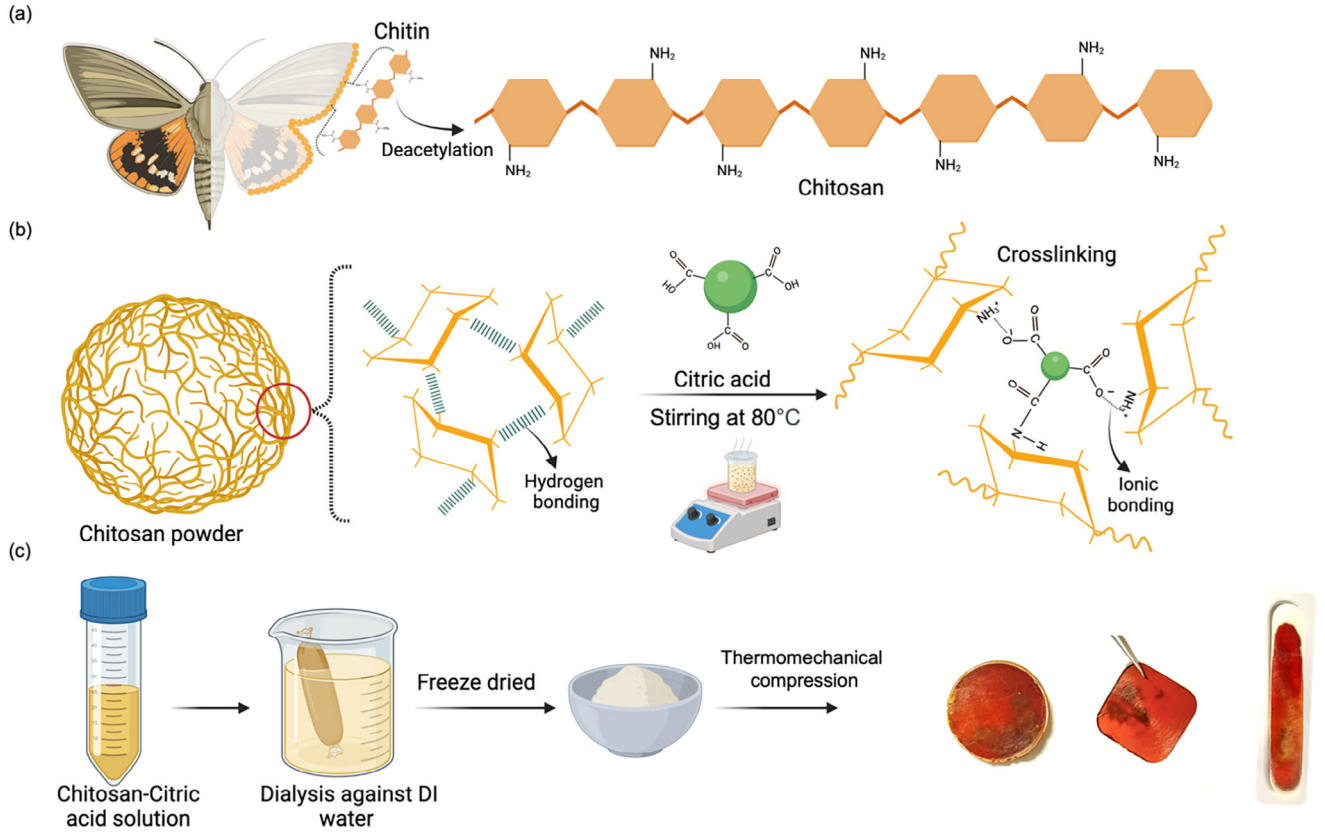

Figure 1. Overview of chitin/chitosan processing. a) Chitin naturally sourced and chitosan as a chemical derivative after deacetylation; b) Chitosan (medium molecular weight (≈200 KDa) cross-linking with citric acid, green ball with exposed carboxylic groups; c) Preparation of chitosan-based dense plastics: step 1 - dialysis of chitosan-citric acid solution against DI water with dialysis membrane M_w cut off: 3.5 kDa; step 2 - freeze drying to generate Cs-CA powder; step 3 – thermomechanical compression for the densification of the powder into plastics (Figure created with Biorender.com).

characterization. The solid state ^{13}C nuclear magnetic resonance (NMR) spectroscopy was carried out for the commercially supplied chitosan and the Cs-CA powder to study the structural changes at the molecular level. The solid state ^{13}C NMR spectra in Figure 2l, revealed characteristic peaks for citric acid and chitosan. The spectrum for Cs-CA powder consisted of peaks corresponding to chitosan structure along with the new peaks ascribed to citric acid. The new peaksat 179.42 ppm and at 45 ppm correspond to the carbon atoms from the citrate ions and significant changes were observed for the peaks corresponding to C1, C4, and C6 of the glucosamine unit of chitosan, where the peaks shifted upfield due to the presence of citric acid in the Cs-CA powder.[27,28] The peak broadening due to citric acid incorporation into chitosan structure can be ascribed to the cross-linking[29] while the peak movement is expected to be due to ionic and covalent interaction between chitosan chains and citric acid.[30] The NMR spectrum for Cs-CA powder was further compared with the spectra obtained for the prepared positive control (Ethylcarbodiimide hydrochloride (EDC) mediated covalent coupling of citric acid and chitosan) and thermomechanically compressed chitosan plastics (Figure S4, Supporting Information). The appearance of peaks and peak shifts for Cs-CA in comparison to chitosan indicated molecular binding of citric acid to chitosan chains during the preparation of Cs-CA, which is therefore not removed during dialysis due to being electrostatically and covalently cross-linked to the chitosan as further confirmed by the X-ray photoelectron spectroscopy (XPS). High resolution N1s XPS scans were obtained for chitosan and Cs-CA powder(Figure 2m). The nitrogen scans revealed the chemical state of nitrogen atoms present in the chitosan in the negative control,Cs-AA, chitosan dissolved in acetic acid, and the changes during Cs-CA preparation. For chitosan, the nitrogen is present mainly as primary amine groups (NH_2) at ≈399 eV.[31] For Cs-CA, new peaks appeared at ≈400.5 and ≈401.3 eV which were ascribed to CO-NH (amide bond) and protonated amines (NH_3^+), respectively. The percentage ascribed to amides was found to be 29%, confirming the amide linkage formed between carboxylic and amine groups.[32,33] The detailed analysis of N1s spectra for the Cs-CA powder when compared with the positive control and the effect of thermomechanical compressing of Cs-CA powder on the amidation was evaluated and presented in Figures S5 and S6 (Supporting Information). The C1s scans (Figure 2n) further revealed the cross-linking between citric acid and chitosan where the peak areas for C—N and C═O increased significantly for Cs-CA in comparison to chitosan in negative control (Cs-AA). The peaks at 286 and 288 eV can be ascribed to the amidation and/or ionic cross-linking between citric acid and chitosan and presence of citric acid, respectively, in Cs-CA.[34] The C1s scans for positive control and Cs-CA samples were compared along with the possible change in the chemical state during thermal processing

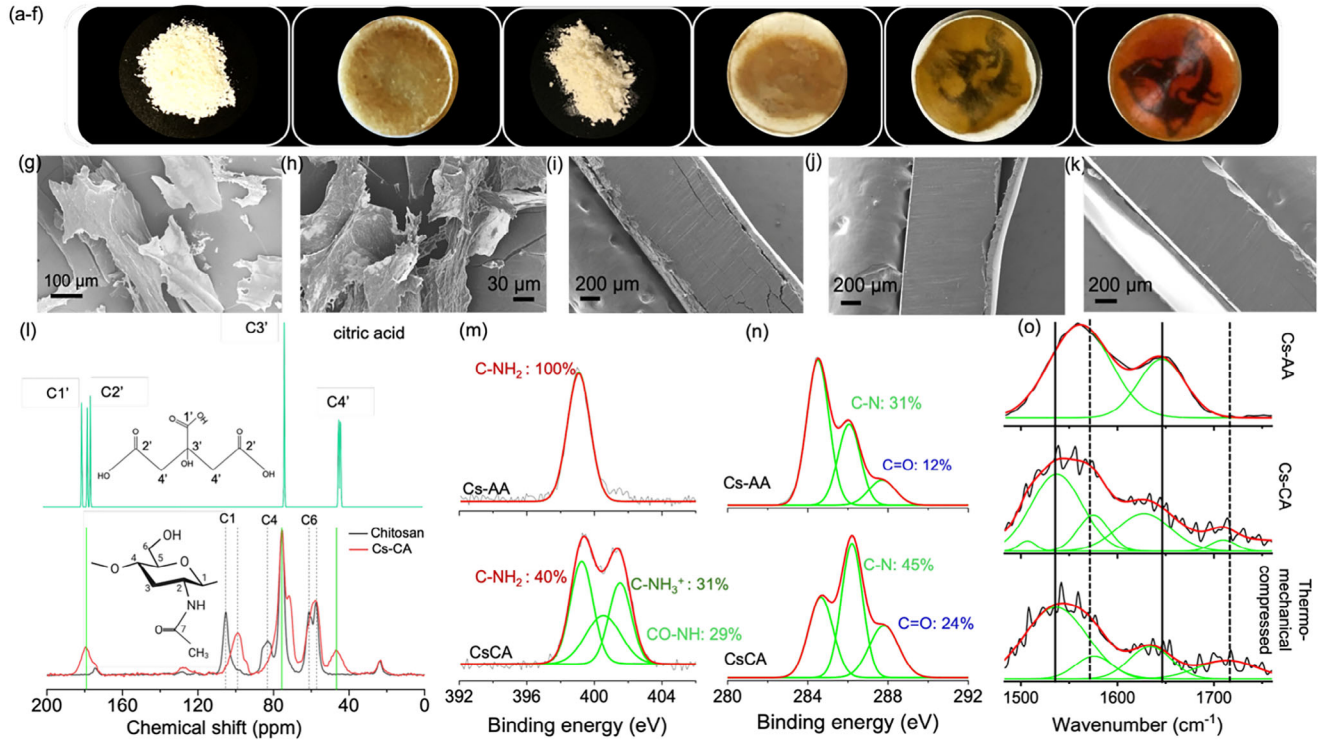

Figure 2. Photographs of: a–f) chitosan powder; chitosan powder thermomechanically compressed at 125 °C; Cs-CA lyophilized powder; chitosan plastic prepared at 60, 90, and 125 °C (from left to right, Tufts' logo in the background to show the optical clarity of the plastics), SEM micrographs: g,h) Cs-CA powder; i–k) cross section of the plastic prepared at 60, 90, and 125 °C; l) solid state ^{13}C NMR spectra of citric acid, chitosan and Cs-CA (inset shows the molecular structure of chitosan and citric acid next to their corresponding ^{13}C NMR spectrum; dotted lines present the peaks for the carbon atom in the glucosamine unit of chitosan and solid line indicate the appearance of the peaks owing to the incorporation of citric acid in the glucosamine chains); m) high resolution N1s XPS spectra of chitosan in acetic acid, Cs-AA, (negative control) and Cs-CA powder; n) high resolution C1s XPS spectra of chitosan in acetic acid, Cs-AA (negative control) and Cs-CA powder; o) FTIR spectra of chitosan in acetic acid, Cs-AA, (negative control), Cs-CA and chitosan plastic prepared at 125 °C.

detailed in the supplementary information (Figures S7 and S8, Supporting Information). To further validate the cross-linking, the free primary amine group content was measured for Cs-CA powder and compared with the positive and negative control; using the trinitrobenzenesulfonic acid (TNBSA) assay where the free amine group concentration was estimated to be reduced to ≈65% for the Cs-CA solution (Figure S9 and Table S2, Supporting Information). The Fourier transform infra-red (FTIR) was performed to gain insight into changes in the molecular structure of chitosan. In Figure 2o, the spetra for the negative control, Cs-AA and the Cs-CA powder showed the changes in the inherent functional groups of chitosan due to presence of citric acid. The FTIR spectrum for the Cs-AA powder showed peaks at 1550 and 1648 cm^{-1} which correspond to the N—H bending/C—N stretching (amide II) and C═O stretching (amide I), respectively, for chitosan.[35] For the Cs-CA sample, the FTIR spectrum demonstrates the presence of peaks at 1505 and 1537 cm^{-1} confirming the presence of both amide II and protonated amines in the samples[35] while the shift of the peak at 1648 to ≈1630 cm^{-1} suggests hydrogen bonding involving the carbonyl group.[36] The broadening of the peak centered at 1550 cm^{-1} hints at overlapping of multiple amide/amine modes suggesting the formation of cross-linked structure. The presence of a peak at 1700 cm^{-1} corresponding to carboxylic acids (C═O stretching vibrations for esters) indicated the presence of citrate ions in the Cs-CA freeze dried and thermomechanically compressed chitosan plastic.[35] For thermomechanically compressed chitosan plastic, the peak at ≈1505 cm^{-1} disappeared which indicates the reduction in the protonated amines which aligns with the XPS scans (Figure, S5, Supporting Information). The detailed FTIR spectra comparison for thermomechanically compressed Cs-CA powder at different processing temperature has been provided in the supplementary information (Figure S10, Supporting Information).

2.3. Structural and Thermal Characterization

The effect of citric acid cross-linking on the crystallographic structure of chitosan was analyzed using X-ray diffraction. Here, the diffractogram for commercial chitosan (Sigma-Aldrich, Burlington, MA, USA) and Cs-CA powder is plotted and compared for possible changes in the diffraction peaks and crystallinity. Inherently, chitosan is partially crystalline as determined by the inter and intramolecular hydrogen bonding between the amino groups and hydroxyl groups.[37] The cross-linking between the partially deacetylated glucosamine chains was carried out by citric acid, as confirmed in the previous section, and its incorporation within the polymeric structure is assessed here. From the

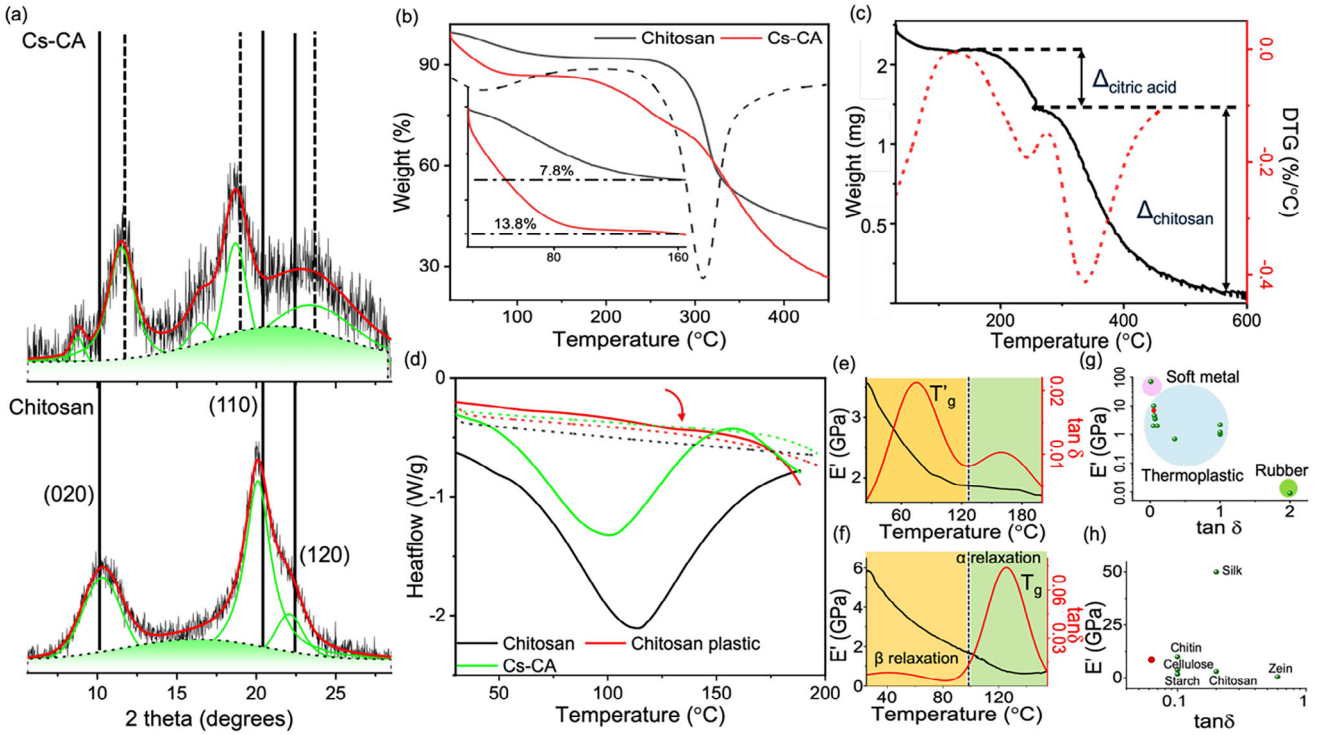

Figure 3. a) X-ray diffractogram of chitosan and Cs-CA powder; b) TGA curve for chitosan and Cs-CA powder and derivative thermogravimetric (DTG) curve of chitosan; c) Modified TGA and DTG curve for Cs-CA powder; d) DSC thermograms of chitosan, Cs-CA powder and chitosan plastic prepared at 125 °C; e) Storage modulus and loss factor for pure chitosan powder thermomechanical compressed at 125 °C; f) Storage modulus and loss factor for Cs-CA thermomechanically compressed at 125 °C; g) Storage modulus and loss factor for different type of materials (red circle presents this work) (details of the materials in the supplementary section, Table S3, Supporting Information); h) comparative plot for storage modulus and loss factor for the films prepared using different biopolymers (red circle presents this work).

comparative plot, **Figure** 3a, the partially crystalline structure of chitosan was confirmed by the presence of two major diffraction peaks at $2\theta \approx 10°$ and $2\theta \approx 20°$. The peak at $2\theta \approx 10°$ was assigned to the hydrated crystals, due to the presence of water molecules in the lattice while the latter peak at $2\theta \approx 20°$ was attributed to the regular crystal lattice structure where chains crystallize in an orthorhombic unit cell.[17,38] We also observed a shoulder peak at $2\theta \approx 22.5°$ for the semicrystalline structure of chitosan which is indexed to (120) planes and reported to arise from partially ordered regions of the polysaccharide chains[39,40] while the amorphous halo is also observed routinely in the pure chitosan samples.[41]

The d-spacing, which represents the distance between the axial repeats for hydrated and anhydrous chitosan (Type I), is calculated to be ≈8.8 Å and agrees with the values obtained in previous works.[28,42] The crystallinity index (CI) for the pure chitosan was determined using peak deconvolution (area) method and calculated to be 0.70 which corresponds to ≈80–85% degree of deacetylation(which was determined from the XPS data, Figure S11, Supporting Information) and has also been reported in previous findings.[43] The CI obtained was confirmed based on these previous findings.[43] Upon cross-linking with citric acid, the diffraction peaks were observed at $2\theta \sim 8.8°$, 11.5°, 16.3°, 18.5°, and 23.8°. The observed peaks shifted with broadening indicative of disordered structures due to the modification of the inter- and intra-hydrogen bonding due to the cross-linking with citric acid.[36,44] The appearance of new peaks can be attributed to the formation of partially ordered structures within the cross-linked chitosan, which has also been reported in the previous findings.[17,45]

The crystallinity index for the Cs-CA powder was calculated to be 0.38, which further confirmed the reduced crystallinity of chitosan based on the incorporation of citric acid. The d-spacing for the prepared Cs-CA powder was decreased to 7.75 Å in comparison to 8.8 Å for pure chitosan indicating the reduced spacing between the chains due to cross-linking.[28] The XRD patterns for the chitosan plastics prepared at 60, 90, and 125 °C show the amorphous nature of the prepared bulk dense materials upon thermomechanical compression (Figure S12, Supporting Information).

The effect of citric acid as a cross-linker and plasticizer and the changes in the thermal property of chitosan upon citric acid incorporation was assessed using thermogravimetric analysis (TGA) and differential scanning calorimetry (DSC) measurements. From the thermogravimetric analysis (inset of Figure 3b), the water content in the Cs-CA powder was 13.8 wt.% which was significantly higher in comparison to that observed for chitosan powder (7.8 wt.%). From the curve, the weight loss for the chitosan powder without citric acid commenced at ≈250 °C, ascribed to the decomposition of the crystallized structure with the maximum weight loss centered at 300 °C.[46] For the citric acid containing samples, Cs-CA powder, the physical and covalent cross-linking between carboxylic and amine groups, as confirmed in

the previous section, was expected to reduce the crystallinity of chitosan.

The derivative thermogravimetric (DTG) curve (Figure 3b) for chitosan showed two peaks at ≈63.5 and 314 °C, corresponding to water loss and chitosan degradation, respectively.[35] In case of Cs-CA powder, the maximum weight loss peak for chitosan shifted toward higher temperature (≈345 °C) which indicated improved thermal stability with incorporated citric acid. The introduction of cross-linker, citric acid, led to interconnected networks of chains leading to delay in the thermal degradation temperature.[47] In the DTG curve for dialyzed Cs-CA (Figure 3c), peaks corresponding to citric acid and chitosan degradation were observed at 243 and 345 °C, respectively, and therefore the TGA analysis procedure was modified to estimate the molar ratio of citric acid with chitosan in Cs-CA powder. In the modified method, the sample was heated to 250 °C and kept in the isothermal condition until the citric acid was completely degraded followed by complete degradation of chitosan. The weight difference was used to calculate the molar content of citric acid and chitosan and molar ratio was estimated to be ≈300 moles of citric acid per mole of chitosan. Furthermore, the effect of citric acid as a plasticizer on chitosan was analyzed using DSC by investigating the glass transition temperature (T_g). The thermogram, Figure 3d, for chitosan powder exhibited an endothermic peak at ≈124 °C which was missing in the thermogram obtained for second heating and therefore was ascribed to the evaporation of moisture in the chitosan powder and referred as the water associated glass transition temperature (T_g').[48] In the cross-linked Cs-CA samples, the thermogram for the first heating showed the water associated endotherm peak centered ≈100 °C which confirmed the reduced glass transition temperature, T_g'. However, there was an onset of another peak at ≈200 °C for the Cs-CA powder which was also observed in the second heating. A similar trend was observed for the Cs-CA samples thermomechanically compressed at 125 °C where the water associated peak disappeared due to the evaporation of the water during processing. There is a minor deflection observed at ≈125 °C for the prepared chitosan plastics, marked by an arrow in Figure 3d which is explored in the next section. The second endotherm peak for Cs-CA powder and prepared plastic was found at ≈200 °C, which could be due to the shifted melting point peak of citric acid. However, the melting point of citric acid occurred at ≈153 °C, which could be shifted to higher temperatures due to the cross-linking with chitosan.[17] The peak at ≈200 °C can also be ascribed to the glass transition temperature for the citric acid cross-linked chitosan which is assumed to partially amorphous due to the cross-linking.[49] The phase transition and material properties of the prepared chitosan plastics was detected using dynamic mechanical analysis, DMA.[50] In the present work, DMA was carried out in the 3-point bending mode to comprehend the viscoelastic and glass transition temperature (T_g) for chitosan plastics. The storage modulus, E', represents the elasticity of the material and exhibits the temperature-dependent behavior when the material transitions from glassy to the viscous/liquid state. In addition to storage modulus, the loss factor/ damping factor of the samples, tan δ, was also assessed and is defined as the ratio of the amount of energy dissipated by viscous mechanisms relative to the energy stored by the elastic component. For the control samples, pure chitosan powder was thermomechanically compressed at 125 °C and the prepared bar was analyzed for its viscoelastic properties. For pure chitosan bars, Figure 3e, the storage modulus was as high as 3 GPa at lower temperature and gradually decreased with increasing temperature, followed by a plateau until 200 °C, while the damping factor, which dictates the glass transition temperature, indicated a peak at ≈80 °C which can be attributed to the β-relaxation from the movement of the local side chains on the chitosan.[51,52] Ordinarily, β relaxation peaks exhibit strong dependency on the water content of the sample and arise due to water absorption from the polymer matrix, therefore, for the present work, the water content of the prepared chitosan bars was estimated to be ≈8 wt.% using TGA (Figure S13, Supporting Information). The absorbed water hydrogen bonds to hydroxyl and amine groups along the polymer chain and takes part in the localized motion within the polymeric chains, which giving rise to the β relaxation. The other tan δ peak was observed at ≈160 °C which can be ascribed to the α relaxation or glass transition due to the motion of segments in the main chain arising from the relaxation of two glucopyranose rings via the glucosidic oxygen and assisted by cooperative hydrogen bonds reordering.[53] In case of the chitosan plastic made from Cs-CA powder prepared at 125 °C, Figure 3f, the storage modulus increased to 6 GPa, in comparison to chitosan plastic made from pure chitosan powder, which indicates the increased stiffness of the plastic due to limited chain mobility due to cross-linking with citric acid. A similar trend was observed for other polymers with increased hardness due to cross-linking.[54–57] Further, the transition region from glassy to liquid state was marked with sharp decline in E' and high damping due to micro-Brownian motion in molecular chains. In the case of the glass transition, the water associated relaxation peak was absent in the chitosan plastic due to absence of significant water content in the plastic as confirmed by TGA (Figure S13, Supporting Information). However, the loss factor (tan δ) peak at 120 °C was due to the primary relaxation and defined as the glass transition temperature which also coincides with the peak observed in the DSC thermogram obtained for Cs-CA plastic, Figure 3d. The reduced T_g and increased loss factor in comparison to pure chitosan plastic was attributed to the plasticization effect of citric acid on chitosan which allows free movement and increased free volume.[58] However, the loss factor was 0.06 (<1) which indicates that the prepared chitosan plastic was predominately elastic. Therefore, from the data, we conclude that citric acid modified the thermal and mechanical properties of the chitosan as a plasticizer and cross-linker.[59] The viscoelastic parameters using DMA of the prepared chitosan plastics was further used for comparison with the existing material forms such as metals, thermoplastics and rubber (Figure 3g).[59–68] The prepared plastic can be categorized as a thermoplastic based on its stiffness and damping factor. Further Figure 3h shows the plastics prepared from Cs-CA plotted with the materials prepared with other biopolymers.[17,69–73] The low loss factor confirmed its superior elasticity in comparison to the films made with the other polymers.

2.4. Tunable Mechanical Properties and Water Uptake

Three-point bending was used to determine the mechanical properties of the bulk chitosan materials with increasing processing temperatures. The chitosan plastics were prepared as cuboid bars

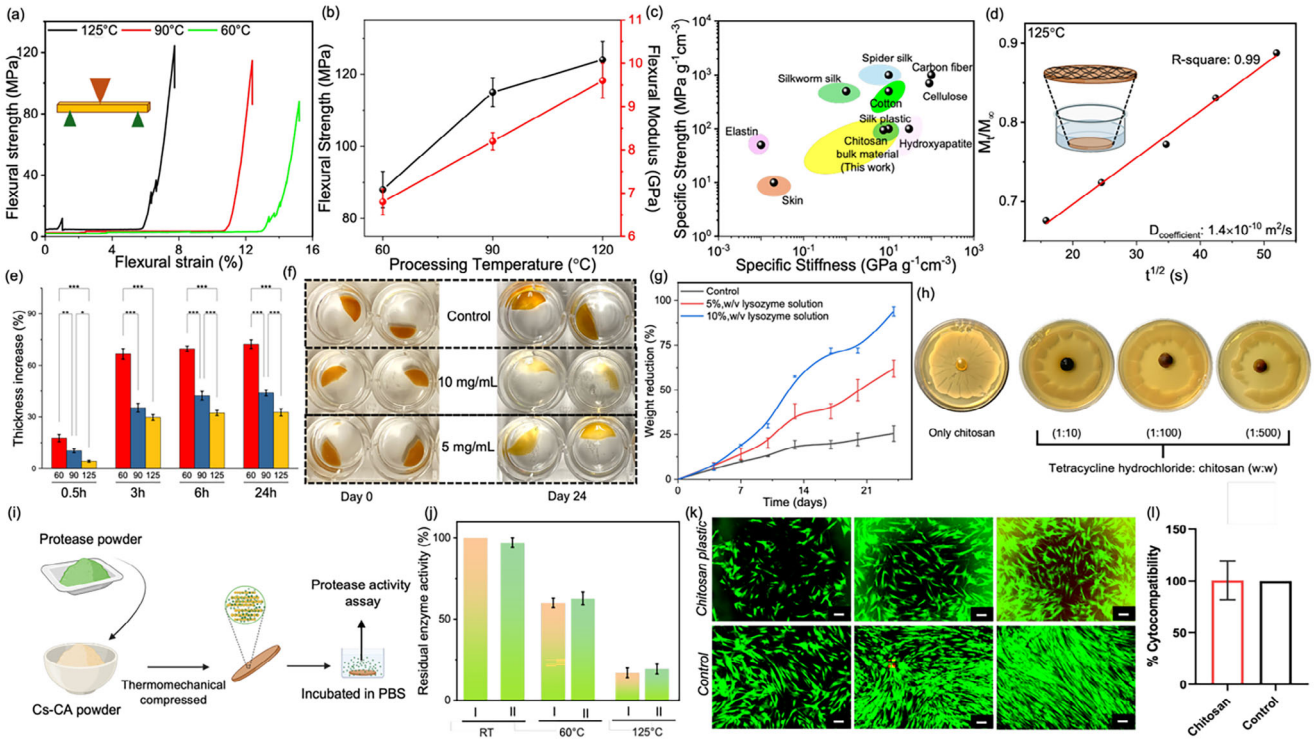

Figure 4. Mechanical properties and aqueous stability based on processing conditions. a) Three-point bending curves for chitosan bars prepared at different temperatures; b) flexural strength and elastic modulus of the chitosan bars prepared at different temperatures; c) comparison of the mechanical properties of the bulk chitosan materials with other natural and synthetic structural materials; d) Fickian diffusion plot fit for the water uptake study for chitosan plastic (schematic shows the cross-linked chitosan plastic in 1X PBS solution); e) comparison plot for increase in thickness of the chitosan plastics based on processing temperature (* $p <= 0.05$,** $p <= 0.01$,*** $p <= 0.001$); f) photograph of chitosan plastics in vitro degradation by lysozyme solution; g) degradation plot for chitosan plastics upon lysozyme treatment; h) antimicrobial activity of tetracycline - no inhibition zone for chitosan plastic, and a clear zone of inhibition formed around the antibiotics containing chitosan materials on the bacteria lawn of Gram positive *Bacillus pasteurii* (left to right); i) schematic for biofunctionalization of chitosan plastic by incorporating protease in chitosan plastic; j) comparative plot for the protease activity profile - I: free protease, and II: protease doped chitosan plastic; RT: room temperature k) live/dead assay of human MSCs for chitosan plastics and control (tissue culture plastic) - scale: 100 µm; l) MTT assay of human MSCs for chitosan plastics and control.

($l = 29\ mm$, $b = 5\ mm$, and $h = 0.8\ mm$) and were placed on two supports and deformed by a centrally positioned load at constant displacement rate of 2 mm min^{-1}. **Figure** 4a shows the flexural stress versus strain plot for bars prepared at 60, 90, and 125 °C. The plots were used to determine the flexural strength and flexural modulus of the prepared plastics; flexural strength is the maximum load the material withstands before it is permanently deformed while flexural modulus indicates resistance to bending or deformation.[74] For the present study, bending strength increased with increased processing temperature, and a similar trend was also seen for flexural modulus (Figure 4b). Since the strength and resistance to deformation for a material are significantly impacted by atomic packing, the density of the chitosan bulk material increased up to 33% when the processing temperature increased from 60 to 125 °C (Figure S14, Supporting Information). The denser plastic hints at the compact packing of the material with increasing temperature which is also demonstrated with the SEM micrographs in Figure 2i–k, where cross sections of the chitosan plastics prepared at 125 °C contained homogeneous features and compact structures in comparison to the samples prepared at 60 °C. Further, we observed a significant darkening in color for the plastics prepared at 125 °C (Figure 2d–f) indicating the increased cross-linking and Maillard-like reactions between amino groups of chitosan and carboxylic groups of the citric acid as confirmed by spectroscopic examination in the previous section.[15] The enhanced networks between polymeric chains resulted in a tough (higher flexural strength) and more resistant to bending (high flexural modulus) material. The specific strength and stiffness of the chitosan bulk materials processed at 125 °C is plotted and compared with those of existing natural and synthetic polymers (Figure 4c).[75,76] The maximum strength for chitosan bulk material is comparable to other materials.[76] The effect of processing pressure on the flexural strength and flexural modulus of the plastics was also assessed and shown in the supplementary section (Figure S15, Supporting Information).

The effect of processing conditions on in vitro water uptake and/or water stability of the chitosan bulk materials was determined using chitosan plastics prepared with different processing conditions (60 and 125 °C – both at 632 MPa). The chitosan plastics were incubated in 1X PBS solution at 37 °C and the increase in weight and dimensions were monitored over time.

The water uptake by the chitosan plastics and the increase in weight was fitted with the Power-law model.[77] The fitted curve is shown in the supplementary information, Figure S16 (Supporting Information). The diffusion exponent indicated the transport

mechanism of water in the plastic was calculated to be 0.45 and 0.5 for the chitosan plastics prepared at 60 and 125 °C, respectively. The values for the diffusion coefficient suggest the Fickian diffusion for water uptake. The effective diffusion coefficient (D_{eff}) for the chitosan plastics was measured using Fick's second law applied to the short-time water uptake data. The Fickian diffusion plot (Figure 4d) for the chitosan plastic prepared at 125 °C showed a diffusion coefficient of 1.4×10^{-10} m^2 s^{-1} in comparison to the diffusion coefficient value of 2.2×10^{-10} m^2 s^{-1} for the plastic prepared at 60 °C (Figure S16, Supporting Information). The observed lower effective diffusion coefficient for the chitosan plastic prepared at 125 °C indicates structural restriction of water movement due to the increase in the cross-linking at the higher processing temperature (as confirmed by XPS and FTIR).

In a similar manner, the thickness of the plastics was also measured during incubation with 1X PBS solution at 37 °C (Figure 4e). The increased thickness followed a similar trend as that of water uptake where the thickness increased to ≈60% for plastics prepared 60 °C in comparison to ≈30% for plastics processed at the higher temperatures (90 and 125 °C). The water uptake and thickness increases were used to determine the porosity of the chitosan bulk materials when processed at different temperatures. The chitosan plastics in the form of pellets, processed at 60, 90, and 125 °C, were incubated in 1X PBS solution and the volume of wet and dry chitosan plastics was calculated to estimate porosity. The samples thermomechanically compressed at lower temperature, i. e., at 60 °C, were more porous ($\Phi = 0.67$) in comparison to a porosity of ≈0.4 for samples processed at 90 and 125 °C.

2.5. In Vitro Degradability and Bio-Functionalization of Chitosan Bulk Materials

Chitosan, as a polysaccharide, is susceptible to degradation when treated with lysozyme which targets the beta-glycosidic linkage between monosaccharides.[78] The in vitro degradability of the chitosan plastics was assessed with lysozyme (Figure 4f) that resulted in the gradual dissolution of the plastics. The mass loss for the plastics is plotted with respect to time when treated with 5% and 10%, w/v lysozyme solution (Figure 4g). Degradation for 25 days revealed up to 100% mass loss for the chitosan-plastics (≈80 mg) incubated in 10%, w/v lysozyme solution, while for the chitosan-plastics in 5% w/v lysozyme solution, ≈50% mass loss occurred. The enzyme solution was replenished every 3rd day for 10% and 5% w/v lysozyme solution. Previous studies on the in vitro degradability of chitosan-based materials such as hydrogels and films with lysozyme have shown a higher rate and extent of degradation in comparison to that for these new thermoplastics (present work).[79–81] Additional details are provided in the supplementary information (Tables S4 and S5, Supporting Information). The increased resistance to enzymatic degradation can be attributed to the denser matrix achieved via thermoplastic molding in comparison to cast films or hydrogels.[82] The chitosan plastics were also doped with lysozyme and monitored for the possible mass degradation by the encapsulated lysozyme which was assessed through mass loss and SEM micrographs (Figures S17–S19, Supporting Information).

To further explore bio-functionalization of the chitosan plastics, they were doped with an antibiotic, tetracycline hydrochloride, to fabricate antimicrobial Cs-CA plastics. The tetracycline powder was mixed with Cs-CA powder in weight:weight ratios of 1:10, 1:100, and 1:500 (tetracycline hydrochloride: Cs-CA powder) and thermomechanically compressed at 125 °C at 632 MPa. The chitosan-tetracycline plastics were assessed for antibacterial activity against Gram positive *Bacillus pasteurii*. The chitosan plastics (controls without antibiotic) did not show growth inhibition of the bacteria (Figure 4h) as no inhibition zone was observed when the plastics were placed on the bacterial lawn. However, for the tetracycline doped chitosan plastics, a zone of inhibition was observed (Figure 4h, left to right). The presence of this inhibition zone confirmed the preservation of the antibiotic activity during the thermomechanical compression at 125 °C. Further, the retention of the activity of biomolecules, incorporated inside the bulk chitosan plastics, was assessed by doping the chitosan-plastics with protease XIV powder and investigating enzyme activity when processed at different temperatures (Figure 4i). The comparative plot, Figure 4j, demonstrates the residual protease activity released from the chitosan plastics into the PBS solution. The protease-doped chitosan plastics were thermomechanically compressed at 632 MPa at 60 °C and 125 °C for 20 min and incubated in 1X PBS solution to evaluate enzyme release from the plastics. Residual enzyme release was 62% and 20% (total enzyme activity estimated for the released protease/ total enzyme activity estimated for the incorporated protease) for the plastics prepared at 60 and 125 °C, respectively. The chitosan plastics fabricated at 60 °C exhibited a mechanical strength of ≈90 MPa, compared to 125 MPa for those processed at 125 °C, Figure 4a. For applications involving biomolecule incorporation, plastics prepared at 60 °C provide sufficient mechanical robustness to withstand potential operational stresses. Furthermore, protease-doped chitosan plastics thermomechanically compressed at room temperature under 632 MPa pressure showed no measurable loss of enzymatic activity. To further evaluate their stability, these room-temperature-processed plastics were incubated in a humidity chamber (80% relative humidity) for two weeks. The samples exhibited no significant changes in either dimensions or weight during this period, confirming their structural stability. Overall, room-temperature-processed chitosan plastics demonstrate excellent enzyme retention, structural stability under high humidity, and suitability for applications requiring long-term storage under less stressful environmental conditions, Table S6 (Supporting Information). The release profile of the protease-doped chitosan plastics was compared with that of pure protease XIV powder, both processed under the same pressure and temperature conditions. For the pure protease XIV powder, there is a retention of 60% w/w and 17% w/w enzyme activity when processed at 60 and 125 °C which aligns with the profile observed for protease-doped chitosan plastics. The results confirm the preparation of bioactive chitosan bulk materials with tunable activity. The controls, consisting of chitosan plastics without enzyme and chitosan plastics doped with inactivated protease (via autoclaving the protease solution) were also incubated in the PBS solution and demonstrated no protease activity. The cytocompatibility of the chitosan plastics was evaluated with human mesenchymal stem cells (MSCs) (Figure 4k), where live/dead imaging demonstrated optimum cell viability with fluorescent cells.

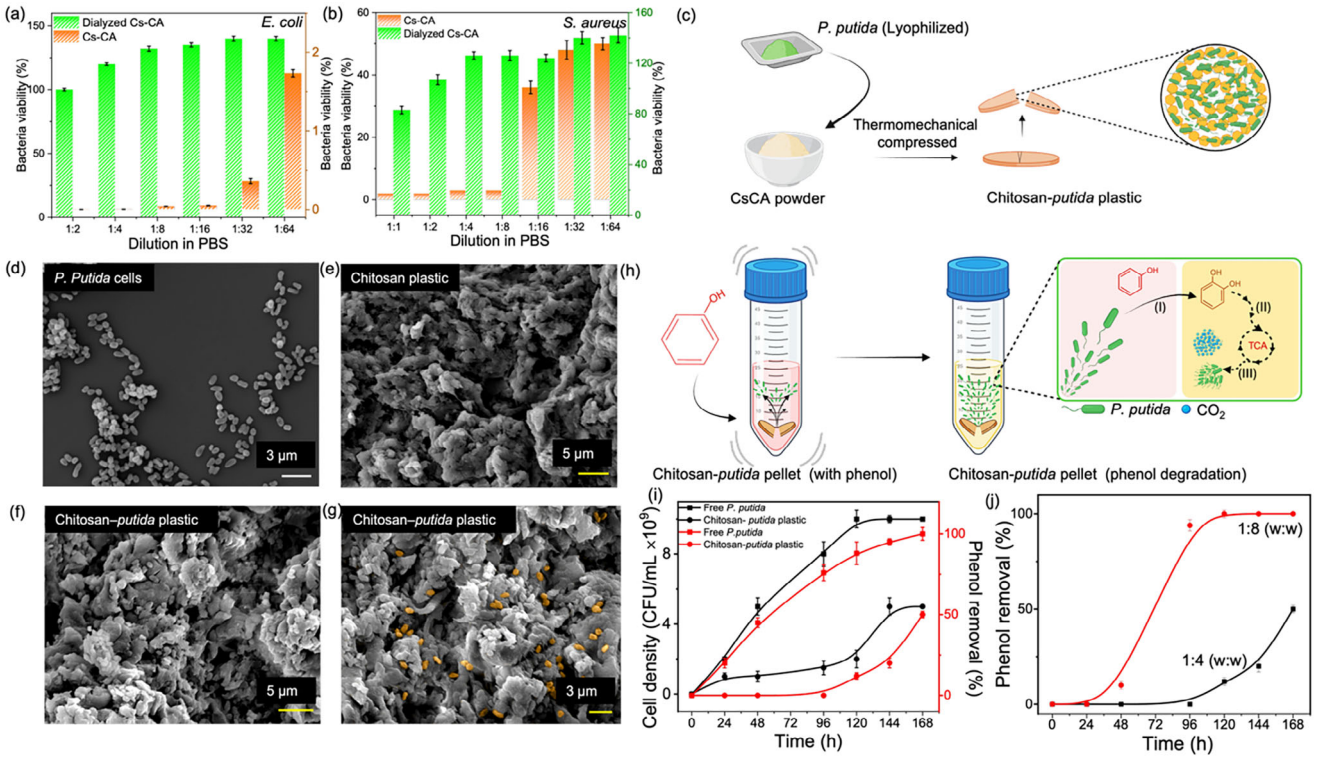

Figure 5. Chitosan plastics as the bacteria containing living materials. a,b) Bacteria viability for *E. coli* and *S. aureus* when incubated with pre and post dialysis Cs-CA solution; c) schematic for the preparation of chitosan-*putida* plastic; d) SEM micrograph of *P. putida* cells, created with Biorender.com; e) SEM micrograph of chitosan plastic; f,g) SEM micrograph of chitosan-*putida* plastic showing the bacteria (identified with the orange color); h) schematic of phenol degradation by the encapsulated *P. putida* cells in the chitosan plastic: chitosan-*putida* plastic was incubated in an MM with phenol as carbon source (mechanism of phenol degradation: (I) phenol conversion into catechol, (II) catechol undergoing metabolic pathways to produce the metabolites entering the TCA cycle, (III) the bacterial biomass and CO_2 synthesis from the intermediates of TCA cycle) (created with Biorender.com); i) Bacterial cell density (CFU/mL) and phenol removal (%) are shown as a function of time for the chitosan-*putida* plastic and an equivalent free bacteria concentration as control; j) phenol removal (%) as a function of time for 1:4 and 1:8, phenol: bacteria weight in the chitosan plastic ratio.

The cell viability assay, Figure 4l, with the 24-h extracts from the thermomechanically compressed chitosan plastics demonstrated enhanced cell proliferation and cell metabolic activity, with cytocompatibility close to 100% (compared to monolayer controls). The AlamarBlue results are provided in Figure S20 (Supporting Information).

2.6. Chitosan Plastics as Living Materials for the Bioremediation of Phenol

Chitosan-based materials ordinarily find their applications as antimicrobial agents due to cationic amine groups which bind to cell surfaces and inhibit microbial growth.[3] However, in the present study, the chitosan plastics demonstrated no significant antibacterial activity (Figure 4h), confirmed by the absence of zone of inhibition when placed on a lawn of *B. pasteurii* bacteria. The lack of antibacterial activity suggests the absence of cationic amine groups, NH_3^+, in the chitosan plastics. To understand the role of NH_3^+ groups in the antimicrobial activity of chitosan, we tested the viability of Gram positive and Gram negative bacteria when incubated with the Cs-CA solution pre- and post-dialysis (when the excess citric acid is removed and the charge density is reduced as confirmed by the zeta potential study, Table S1, Supporting Information). The viability of Gram positive *S. aureus*, detected using AlamarBlue, was presented in **Figure 5a**, where high bacterial viability was found for the samples incubated with dialyzed Cs-CA solution in comparison to the low bacteria viability when incubated in the pre-dialysis Cs-CA solution. The same trend was observed for Gram negative *E. coli* (Figure 5b), where bacterial viability was significantly higher for samples incubated with the dialyzed Cs-CA solution. The findings confirmed the absence of antibacterial activity in the dialyzed Cs-CA solution, which can be used to prepare bacterial embedded chitosan bulk materials for a range of potential utilities.

To explore the functionality of chitosan-based living materials in degrading toxins, the bacteria-doped chitosan plastics were prepared with lyophilized *P. putida* cells mixed with the Cs-CA powder and thermomechanically compressed at 60 °C, yielding the chitosan-*putida* plastics (Figure 5c). The packing of bacteria inside the plastics was assessed using SEM where the cross section of the chitosan-*putida* material was imaged and compared with chitosan plastics without bacteria as controls. Controls of *P. putida* cells without chitosan, were also imaged using SEM (Figure 5d), and indicated the cells were rod shaped ≈0.5 to 1 µm in length and used as a reference while imaging the bacteria inside the plastics. The control chitosan plastic with no encapsulated bacteria is shown in Figure 5e, while the bacteria-containing

chitosan plastics are shown in Figure 5f,g and demonstrate bacteria cells embedded within the chitosan bulk materials. The SEM images revealed the cells had the same features as the control (Figure 5d). Furthermore, the viability of the cells embedded within the chitosan plastic was estimated using AlamarBlue (Figure S21, Supporting Information), which showed the cells to be 100% viable after thermomechanical processing.

For phenol degradation, the bacteria-containing chitosan plastics were incubated in minimal medium (MM) containing salts with phenol as the carbon source (Figure 5h). The phenol is metabolized by the cells to catechol which is further metabolized to produce substrates that enter the tricarboxylic acid (TCA) cycle.[83,84] The cells metabolize environmentally hazardous phenol into biomass and CO_2. For the present work, the degradation of phenol into biomass was monitored by recording cell density (CFU/ml) and phenol concentration of the medium with time. For a phenol concentration of 500 mg L^{-1}, the phenol removal capability of chitosan-*putida* plastic was compared to free *P. putida* cells as the control (Figure 5i). Phenol degradation by cells encapsulated in the chitosan plastics initiates after ≈96 h of incubation, in comparison to 24 h for free cells. This delay can be ascribed to the longer adaptation period for the cells in the plastic, as a similar trend was followed by the cell density plot hinting at an extended lag phase. The increase in the cell density with phenol degradation indicates the growth of bacteria metabolizing phenol. To rule out the consumption of chitosan by the cells as a carbon source for growth, we incubated *P. putida* cells in the minimal media supplemented with phenol (100 mg L^{-1}) and chitosan plastics (50 mg). The increase in the cell density was estimated using a plate count method and no increase in the cell number was recorded for the cells incubated with the chitosan plastic, confirming the cells were only using phenol for growth. Previous studies on the degradation of phenol by *P. putida* reported phenol removal to be a factor of inoculum size.[85] We attempted to decrease the lag phase for the chitosan-*putida* plastic by doubling the inoculum size in the plastic from 10 to 20 mg of lyophilized *P. putida* cell powder that corresponds to 1:8 (w/w), phenol to inoculum weight ratio. The comparative plot, Figure 5j, shows faster degradation of phenol with an adaptation period of ≈24 h and complete removal of phenol within 196 h for the chitosan-*putida* plastics. A similar trend was also observed when the initial phenol concentration was decreased to 100 mg L^{-1} instead of 500 mg L^{-1}, which resulted in a decreased adaptation period for the chitosan-*putida* plastics and faster removal of phenol (Figures S22 and S23, Supporting Information). The effect of processing temperature on the bacteria release was also studied and shown in Figure S24 (Supporting Information). The reusability of the chitosan-*putida* plastics was assessed by extensively rinsing the chitosan-*putida* plastics in deionized (DI) water and incubating them in the same initial concentration of phenol for a second round of degradation. Here, the phenol was completely degraded, and the degradation time decreased from 96 to 24 h (Figure S25, Supporting Information).

3. Conclusion

A solid-state processing approach for preparing chitosan into chitosan-based bulk, plastic-like materials was demonstrated. In this process, chitosan is solubilized with citric acid, which serves as both a cross-linker and plasticizer, facilitating packing of chitosan into bulk plastics with tailored chemical and physical properties through thermoplastic molding. The thermally processed chitosan plastics exhibited tunable structural and mechanical properties with compatibility with bioactive molecules and living cells (human mesenchymal stem cells and bacterial cells). Furthermore, compatibility with bacterial cells enabled the generation of bacteria-laden chitosan-based living plastics through the encapsulation of *Pseudomonas putida*, known as a phenol degrading organism. The resulting chitosan-*putida* plastics degraded phenol into bacterial biomass, confirming potential for pollutant removal applications using these sustainable chitosan-like plastics. The ease and versatility of thermoplastic processing of these chitosan-based plastics suggests a new generation of functional biomaterials with broad biotechnological applications, as well as a new sustainable approach to functional plastics.

4. Experimental Section

Preparation of Citric Acid Cross-Linked Chitosan (Cs-CA): Cross-linking was carried out by dissolving 2.5% w/v chitosan (medium molecular weight, 19–30 kDa M_w, Sigma-Aldrich, Burlington, MA, USA) in 0.15 M citric acid (Sigma-Aldrich, Burlington, MA, USA) in de-ionized (DI) water by stirring overnight at 80 °C. The prepared Cs-CA solution was filtered through a 70 µm pore size cell strainer (Thermo Fisher Scientific, Waltham, MA, USA) to remove undissolved chitosan particles and subsequently dialyzed for 4 to 5 days in distilled water using dialysis membranes with a membrane molecular weight cut-off of 3.5 kDa. Dialysis continued until no citric acid residue was detected via electrospray ionization mass spectrometry, ESI-MS (Finnigan LTQ, a linear ion trap with ESI, Thermo Fisher Scientific, Waltham, MA, USA). After dialysis, the membrane contents were sonicated in an ultrasonic bath for 2 h to homogenize the Cs-CA gel suspension (optional). The solution was then flash frozen using liquid nitrogen and lyophilized in a freeze dryer (Labconco Corporation, Kansas City, MO, USA)at −80 °C and 600 Pa until complete sublimation. The powder obtained in this process was stored in airtight containers until used for further processing. For the confirmation of citric acid linking to chitosan, a positive control was prepared where citric acid was covalently attached to the chitosan backbone using a covalent coupling agent, 1-(3-dimethylaminopropyl)-3-ethylcarbodiimide hydrochloride (EDC). For the coupling, 2.5 g of chitosan was mixed with 4.0 g of citric acid in 50 mL of DI water followed by drop-wise addition of 50 mL of DI water and ethanol (1:1) containing 4.0 g of EDC (Sigma-Aldrich, Burlington, MA, USA). The reaction solution was stirred overnight at room temperature with the pH maintained at 5.0, followed by dialysis for 3 to 4 days in distilled water with a membrane molecular weight cut-off of 3.5 kDa. For the negative control, Cs-AA, the chitosan (2.5% w/v) was dissolved in acetic acid (1% v/v) (Sigma-Aldrich, Burlington, MA, USA), dialyzed for 4 to 5 days in distilled water using dialysis membranes with a membrane molecular weight cut-off of 3.5 kDa. Dialysis continued and pH of the solution was assessed using pH meter (Fischer Scientific, Waltham, MA, USA) until pH of the solution reached 5 to 6. After dialysis, the solution in the membrane was then flash frozen using liquid nitrogen and lyophilized. The obtained powder was used as negative control for the material characterization.

Thermomechanical Compression of Chitosan: The Cs-CA powder was packed into predesigned molds, followed by compression at 632 MPa at different temperatures (60, 90, and 125 °C) using a hot press (YLJ-HP88V-250, Tmax Battery Equipments, Xiamen, Fujian, China) for 20 min to assess processing windows. After the thermomechanical compression, the samples were cooled to room temperature and characterized.

Scanning Electron Microscopy (SEM): Material morphology was characterized by SEM (Zeiss Ultra 55 field-emission scanning electron microscope (FE-SEM), Zeiss Gemini 560 FE-SEM, Jena, Germany). The SEM images were collected with a voltage of 10 kV, and the samples were

sputter-coated with a 5 nm thin layer of Pt/Pd. For the lyophilized Cs-CA, the powder was imaged, as was the cross section of the plastics compressed at the different temperatures (60, 90, and 125 °C). The cross section was obtained by cutting the plastics using a.024 Deep Cut Ball End Mill with 200″ cut length. For the bacteria-containing plastics and the free bacteria controls, the samples were washed with DI water 2 to 3 times and then fixed with 2% v/v glutaraldehyde (EMS Electron Microscopy Sciences, Hatfield, PA, USA) in 0.1 M sodium cacodylate buffer pH 7.4 (Electron Microscopy Sciences, Hatfield, PA, USA) for 2 to 3 h. Post fixation, the samples were washed with 0.1 M sodium cacodylate buffer and dehydrated using an ethanol gradient (50%, 70%, 95%, and 100% ethanol). The dehydrated samples were dried using a step gradient of hexamethyldisilazane (HMDS) (Electron microscopy sciences, Hatfield, PA, USA) in 100% ethanol. For bacteria samples, the samples were sputter coated with a 10 nm thin layer of Pt/Pd to avoid charging and the SEM images were collected with a voltage of 10 kV.

Nuclear Magnetic Resonance Spectroscopy (NMR): The cross-linking of citric acid to chitosan chains was probed using solid-state ^{13}C NMR (Bruker Avance III HD 600 MHz spectrometer, Bruker BioSpin GmBH, Germany). The analysis was carried out at ^{1}H and ^{13}C frequencies of 600.13 and 150.90 MHz, respectively, in a 4.0 mm cross-polarization and magic angle spinning (CP/MAS) broadband-observe probe. ^{13}C CP/MAS experiments with high-power ^{1}H decoupling were conducted. Recycle delay, contact time, decoupling field, and spinning speed were 3 s, 1 ms, 69 kHz, and 8 kHz, respectively. Spectra were obtained for chitosan powder, citric acid, lyophilized Cs-CA, and thermomechanical compressed Cs-CA. For the thermomechanical compressed Cs-CA samples, the plastics were frozen and milled using BioPulverizer (BioSpec products, Bartlesville, OK, USA) into powder for analysis. The positive control, where citric acid was covalently coupled to chitosan using EDC, was also prepared and compared with the other samples to confirm covalent cross-linking between chitosan chains and citric acid. NMR spectra were processed with TopSpin 3.5 pl 6 software and chemical shifts in parts per million (ppm) are reported.

X-Ray Photoelectron Spectroscopy (XPS): The extent of covalent and ionic cross-linking between citric acid and chitosan chains was analyzed using XPS using an XRA-008, Thermo Scientific K-Alpha+ XPS, Waltham, MA, USA, with a monochromatic Al Kα X-ray source operating at 12.5 kV and 16 mA. The high-resolution scans for carbon and nitrogen atoms, C1s and N1s, were obtained and compared for lyophilized Cs-CA (positive control), Cs-AA (negative control) and the obtained chitosan plastics to identify the functional groups and analyze the presence of amide bonds. The data were analyzed using Origin pro software and deconvolution was carried out using a secondary derivative method with Voigt model selected to improve the resolution and identification of the overlapping spectra peaks.

Fourier Transform Infra-red Spectroscopy (FTIR): FTIR was carried out on a JASCO FTIR 6200 spectrometer (FT/IR-6200, JASCO, Japan) equipped with a MIRacle attenuated total reflectance Ge crystal cell in absorbance mode. For each measurement, the spectrum was recorded with 64 scans and a resolution of 4.0 cm^{-1}. Multiple spectra ($n >= 3$) were collected for Cs-CA powder (positive control), Cs-AA (negative control), and chitosan plastics. For each experimental condition, multiple samples ($n >= 3$) were prepared and characterized. The data were analyzed using Origin pro software and deconvolution was carried out using a secondary derivative method with Gaussian model selected to improve the resolution and identification of the overlapping spectra peaks.

Primary Amine Group Estimation: 2,4,6-Trinitrobenzenesulfonic (TNBSA) assay was used to quantify the primary amine content of the samples. A 0.5 mg mL^{-1} solution of CsCA powder, positive control and negative control (Cs-AA) in 1% v/v acetic acid, was mixed with 0.05% w/v TNBSA solution in 0.2 M $NaHCO_3$ buffer (pH 8.5) at 1:1 volume ratio, incubated at 37 °C for 2 h and its absorption at 420 nm was measured ($n = 5$) using SpectraMax M2 multimode microplate reader. The calibration curve was prepared with known concentrations of β-alanine standard solutions.

Wide Angle X-Ray Diffraction (WAXS): The structural characterization of commercial chitosan powder (medium molecular weight, Sigma-Aldrich, Burlington, MA, USA) and Cs-CA powder was assessed by X-ray diffraction. The data were obtained using a Philips PW 1830 X-ray generator (Panalytical, Almelo, Netherlands). The system provided nickel filtered Cu Kα radiation of wavelength, $\lambda = 0.154$ nm, operated at 30 kV and 55 mA at room temperature, with a diffracted beam graphite monochromator. Samples were mounted on Al sample holders and scans were obtained in $\theta/2\theta$ reflection mode. WAXS intensity plots were recorded at a step scan interval of 0.02°/step with a dwell time of 2 s/step. The scattering angle, 2θ, varied from 5°–40°.

Thermal Analysis: The thermal degradation of Cs-CA powder was measured by thermogravimetric analysis, TGA, from 25 to 800 °C in N_2 (99.99%) with a scanning speed of 5 °C min^{-1}. The TGA was carried out on Discovery TGA 550 (TA Instruments, New Castle, Delaware, USA) where samples were kept under N_2 in the furnace to reach a stable weight prior to heating. Differential scanning calorimetry, DSC, measurements were carried out on Discovery DSC 250 (TA Instruments) under a dry N_2 gas flow of 50 mL min^{-1} with samples encapsulated in aluminum pans. The samples were heated from -50 to 200 °C at a heating rate of 10 °C min^{-1}. Chitosan powder was run as a control for TGA and DSC for comparison.

Dynamic Mechanical Analysis (DMA): The viscoelastic properties of the chitosan plastics (prepared at 125 °C) were measured with a DMA-1 (Mettler Toledo Instruments, Columbus, Ohio, USA) in 3 point bending mode. The samples were prepared in the shape of cuboid bars with a length of ≈29 mm, a width of ≈5 mm and a thickness of ≈1 mm. DMA analysis was carried out with temperature sweeping from 30 to 200 °C, under the following conditions: heating ramp, 3 °C min^{-1}; initial strain, 0.01%; preload force, 0.3 N; and frequency, 1 Hz. The commercial chitosan powder thermomechanically compressed at 125 °C at 632 MPa was used a control for the DMA study.

Mechanical Properties: Three-point bending tests were carried out on an Instron 3366 machine (Instron, USA) in flexural test mode with a loading rate of 1 mm min^{-1}. The specimens were prepared at 60, 90, and 125 °C in the shape of cuboid bars with a length of ≈29 mm, a width of ≈5 mm and a thickness of ≈1 mm. Three samples were evaluated at room temperature for each condition.

Water Uptake: The chitosan plastics (in the shape of discs with a thickness of 1 mm and diameter of 10 mm) were placed 1X PBS solution (Gibco, Fischer Scientific, Waltham, MA, USA) and incubated at 37 °C in an incubator (Thermo Fischer Scientific, Waltham, MA, USA) for various times (0, 60 min, 3 h, 12 h, 24 h, 15 days, 30 days) and the change in weight, thickness, and diameter were assessed for swelling. Surface moisture was removed from the samples by wiping with a Kimwipe (Kimberly-Clark), the wet weight of the sample was determined (Ws) and the thickness and diameters were measured. The water uptake (%) was calculated as follows:

$$\%\text{Water uptake} = \frac{(\text{Wet sample weight} - \text{dry sample weight})}{(\text{dry sample weight})} * 100 \quad (1)$$

In Vitro Degradability: Chitosan plastics were incubated in 2 mL of 5 and 10 mg mL^{-1} of lysozyme (ThermoScientific, Thermo Fisher Scientific, Waltham, MA, USA) solution in PBS at 37 °C to assess enzymatic degradation. The lysozyme solution was replenished every 2–3 days. At the designated time points, the samples were rinsed in deionized water and dried to constant weight before weighing. The Cs-CA powder was doped with lysozyme powder in the weight ratio of 1:1, 1:2, and 1:3 (lysozyme: Cs-CA) and thermomechanically compressed at 125 °C to prepare lysozyme doped plastics. The obtained plastics were incubated inPBS solution at 37 °C to assess their possible degradation.

Antibiotic-Doped Chitosan: Tetracycline hydrochloride (EMD chemicals, Inc. San Diego, CA, USA) was added to the Cs-CA powder in weight ratios of 1:500, 1:100, and 1:10 (tetracycline hydrochloride:Cs-CA) and mixed thoroughly. The resulting mixture was thermomechanically compressed at 125 °C at 632 MPa to obtain the antibiotic doped chitosan plastics. The antibacterial activity of the plastics was assessed for *Bacillus pasteurii* (American Type Culture Collection, ATCC, USA) which was grown on the growth media agar plates containing 2% w/v agar (Thermo Fisher Scientific, Waltham, MA, USA), 20 g L^{-1} yeast extract (Sigma-Aldrich, Burlington, MA, USA), 10 g L^{-1} ammonium sulfate (Thermo Fisher Scientific,

Waltham, MA, USA) in 0.13 M tris buffer (pH: 9) (Thermo Fisher Scientific, Waltham, MA, USA).

Protease-Doped Chitosan: Commercial protease powder (Protease from *Streptomyces griseus* type XIV, Sigma-Aldrich, Burlington, MA, USA) was added to the Cs-CA powder in the ratio of 1:10, w:w (protease XIV: Cs-CA) and mixed thoroughly. The mixture was thermomechanically compressed at 60 and 125 °C at 632 MPa to prepare protease-doped chitosan plastics. The plastics were incubated in PBS solution at room temperature and the protease release in the solution was assessed by estimating the protease activity over time. Protease activity was estimated using the Pierce protease assay (, ThermoScientific, Thermo Fisher Scientific, Waltham, MA, USA). The free protease powder was also processed under similar conditions (60 and 125 °C at 632 MPa) and assessed for enzyme activity.

Cytocompatibility: Human Mesenchymal stem cells (ATCC, USA) were cultured in Dulbecco's Modified Eagle's Medium (DMEM, Gibco, USA) supplemented with 10% Fetal Bovine Serum (FBS, Gibco, USA), 1% Antibiotic-Antimycotic (Gibco, USA), 1% Non-essential Amino Acids (Gibco, USA) and 5 ng mL^{-1} Fibroblast Growth Factor-2 (FGF-2, Peprotech, USA). The cells were allowed to proliferate until 80% confluency. The chitosan plastics were pre-soaked in the media for 24 h, and then 10000 cells were seeded for Lived/dead (Invitrogen, USA), AlamarBlue(Invitrogen, USA), and 2,5-diphenyl-2H-tetrazolium bromide (MTT, Abcam, USA) assays. The cell-seeded plastics on days 1, 7, and 14 were stained with 2 μM Calcein (Live) and 4 μM Ethidium homodimer (Dead) dyes, incubated for 30 min and imaged using a fluorescence microscope (BZ-X700, Keyence, USA). Cell proliferation was analyzed using the AlamarBlue assay, and cell metabolic activity was evaluated using the MTT assay.

Antibacterial Activity: Chitosan provides antibacterial activity due to the abundance of cationic functional groups.[86] The removal of excess citric acid during dialysis reduces the amount of cationic amine groups in the prepared chitosan solution and was expected to mitigate the antimicrobial effects. In this work, the anti-bacterial activity of the CA-Cs solution, pre- and post-dialysis was assessed, against Gram positive and Gram negative bacteria, i.e, *Staphylococcus aureus* and *Escherichia coli*, respectively. AlamarBlue assay was carried out to quantify bacterial viability where 50 μL of the diluted pre- and post-dialysis CA-Cs solutions in PBS were pipetted into 96 well plates and mixed with 50 μL of bacteria culture suspension containing 10^5 cells per mL. The media controls included Luria Bertani (LB) broth (Fischer Bioreagents, NH, USA) and Tryptic Soy broth (TSB) (Sigma-Aldrich, Burlington, MA, USA) for *E. coli* and *S. aureus*, respectively. The plates containing *E. coli* and *S. aureus* were incubated at 37 °C overnight with agitation, followed by the addition of 10 μL of AlamarBlue reagent (Thermo Fisher Scientific, Waltham, MA, USA). The plates were then incubated in dark at 37 °C for 20 min. The fluorescence of the incubated AlamarBlue solutions for *E. coli* and *S. aeureus* was recorded with a microplate reader (Varioskan LUX multimode, Thermo Fisher Scientific, Waltham, MA, USA) with excitation/emission at 560/590 nm. Bacterial viability was calculated using the following formula:

$$\%\ \text{Bacterial Viability} = \frac{(\text{FI of well} - \text{Avg. FI media control})}{(\text{Avg. FI growth control} - \text{Avg. FI media control})} \times 100 \quad (2)$$

where FI = Fluorescence intensity

Chitosan-Based Living Materials for Phenol Remediation: Bacteria culture conditions - A 5 mL starter culture of *Pseudomonas putida* (Trevisan) Migula (ATCC 700007) was grown in 50 mL nutrient broth (NB) medium containing 1 g L^{-1} glucose (Sigma-Aldrich, Burlington, MA, USA), 3 g L^{-1} yeast extract (Sigma-Aldrich, Burlington, MA, USA), 6 g L^{-1} sodium chloride (Sigma-Aldrich, Burlington, MA, USA), and 15 g L^{-1} bacteriological peptone (Thermo Fisher Scientific, Waltham, MA, USA) and incubated for 24 h on an orbital shaker at 150 rpm at 30 °C. To measure the concentration of the *P. putida* culture grown overnight, the culture was centrifuged at 8,000 rpm for 20 min and the optical density (OD) measured at 600 nm using a spectrophotometer (Thermo Fisher Scientific, Genesis 10S) with 0.85% w/v sodium chloride solution as blank.

Chitosan-*putida* plastics preparation and phenol degradation - For the preparation of chitosan-*putida* plastics, the actively growing *P. putida* culture suspension was centrifuged, and the pellet was lyophilized at −80 °C and 0.006 bar until complete sublimation. The lyophilized cells were mixed with Cs-CA powder in different ratios (i.e., 1:5 and 1:2, w:w bacterial cells: CsCA powder). The mixes were thermomechanically compressed at 60 °C, 632 MPa to obtain the chitosan-*putida* plastics. Controls were prepared via thermomechanical compression Cs-CA powder alone and free bacterial cells alone at 60 °C, 632 MPa. For phenol degradation, the samples were incubated in 5 mL of the minimal medium (MM) containing Na_2HPO_4 (5.4 g L^{-1}, Sigma-Aldrich, Burlington, MA, USA), KH_2PO_4 (1.4 g L^{-1}, Sigma-Aldrich), $(NH_4)_2SO_4$ (0.5 g L^{-1}, Sigma-Aldrich), $MgSO_4{\cdot}7H_2O$ (0.2 g L^{-1}, Sigma-Aldrich), and trace mineral supplements (5 mL L^{-1}; MD-TMS, ATCC) supplemented with 100 mg L^{-1} of phenol (Thermo Fisher Scientific) as the sole carbon source. Cell growth (CFU/mL) and phenol degradation were monitored over a week. The cell density was measured using the drop plate method, where the MM medium containing the samples and controls was diluted 10^3 times and 10 μL of the diluted sample was dropped on the NB agar plate. The cell colonies were counted after 6 to 8 hours. Phenol concentrations were determined for both the bacteria-containing plastics and the bacterial controls using a 4-aminoantipyrine spectrophotometric method.[19] Briefly, the minimal medium containing the chitosan-*putida* plastic was centrifuged to remove the released cells and 125 μL of cell-free sample was mixed with 25 μL of 0.1 M glycine buffer (pH 9.7) followed by addition of 62.5 μL of 0.2%, w/v, 4-aminoantipyrine and 50 μL of 0.5% w/v, $Fe(CN)_6$. The absorbance of the red-color solution was measured at 505 nm using a spectrophotometer (Varioskan LUX multimode, Thermo Fisher Scientific, Waltham, MA, USA) and compared to a standard curve.

Statistical Analysis: OriginPro (OriginLab Corporation, Massachusetts, USA) was used for all statistical analyses and all data are shown as the mean ± s.d. unless otherwise indicated. Two-way analysis of variance (ANOVA) with Tukey's post hoc multiple comparison test was used to determine statistical significance ($*p \leq 0.05$, $**p \leq 0.01$, $***p \leq 0.001$). Correlation of two variables were analyzed using simple linear regression test to obtain a linear equation ($R^2 > 0.95$) for calibration curves used in quantification of primary amine contents by TNBSA assay.

Supporting Information

Supporting Information is available from the Wiley Online Library or from the author.

Acknowledgements

The authors thank the AFOSR (FA9550-23-1-0606) and the NIH (P41EB027062) and NSF (DMR-2003629) for support of this work. The authors also thank S. Maccorkle at the Tufts University Machine Shop for materials machining. This work was performed in part at the Harvard University Center for Nanoscale Systems (CNS); a member of the National Nanotechnology Coordinated Infrastructure Network (NNCI), which is supported by the National Science Foundation under NSF award no. ECCS-2025158.

Conflict of Interest

The authors declare no conflict of interest.

Data Availability Statement

The data that support the findings of this study are available from the corresponding author upon reasonable request.

Keywords

biodegradable, bioremediation, Chitosan plastics, living materials, thermomechanical compression

Received: June 19, 2025
Revised: October 7, 2025
Published online:

[1] B. Krajewska, *Sep. Purif. Technol.* **2005**, *41*, 305.
[2] S. Sreekumar, J. Wattjes, A. Niehues, T. Mengoni, A. C. Mendes, E. R. Morris, F. M. Goycoolea, B. M. Moerschbacher, *Nat. Commun.* **2022**, *13*, 7125.
[3] J. Wang, S. Zhuang, *J. Cleaner Prod.* **2022**, *355*, 131825.
[4] F. Korbinian Scharnagl, M. Franz Hertrich, F. Ferretti, C. Kreyenschulte, H. Lund, R. Jackstell, M. Beller, *Sci. Adv.* **2018**, *4*, aau1248.
[5] S. K. Samal, M. Dash, S. Van Vlierberghe, D. L. Kaplan, E. Chiellini, C. van Blitterswijk, L. Moroni, P. Dubruel, *Chem. Soc. Rev.* **2012**, *41*, 7147.
[6] T. Maschmeyer, R. Luque, M. Selva, *Chem. Soc. Rev.* **2020**, *49*, 4527.
[7] E. E. Leonhardt, N. Kang, M. A. Hamad, K. L. Wooley, M. Elsabahy, *Nat. Commun.* **2019**, *10*, 2307.
[8] B. Jia, H. Huang, Z. Dong, X. Ren, Y. Lu, W. Wang, S. Zhou, X. Zhao, B. Guo, *Chem. Soc. Rev.* **2024**, *53*, 4086.
[9] B. Park, J. H. Shin, J. Ok, S. Park, W. Jung, C. Jeong, S. Choy, Y. J. Jo, T. I. Kim, *Science* **2022**, *376*, 624.
[10] W. Tang, J. Wang, H. Hou, Y. Li, J. Wang, J. Fu, L. Lu, D. Gao, Z. Liu, F. Zhao, X. Gao, P. Ling, F. Wang, F. Sun, H. Tan, *Int. J. Biol. Macromol.* **2023**, *240*, 124398.
[11] S. Kumar, R. Dhiman, C. R. Prudencio, A. C. da Costa, A. Vibhuti, E. Leal, C.-M. Chang, V. S. Raj, R. P. Pandey, *Mini-Rev. Med. Chem.* **2022**, *23*, 187.
[12] M. N. Kantak, S. S. Bharate, *Carbohydr. Polym.* **2022**, *278*, 118999.
[13] M. Leonida, P. Ispas-Szabo, M. A. Mateescu, *Bioact. Mater.* **2018**, *3*, 334.
[14] V. K. Thakur, S. I. Voicu, *Carbohydr. Polym.* **2016**, *146*, 148.
[15] A. C. Galvis-Sánchez, A. M. M. Sousa, L. Hilliou, M. P. Gonçalves, H. K. S. Souza, *Green Chem.* **2016**, *18*, 1571.
[16] E. Jakubowska, M. Gierszewska, J. Nowaczyk, E. Olewnik-Kruszkowska, *Food Hydrocoll.* **2020**, *108*, 106007.
[17] P. Guerrero, A. Muxika, I. Zarandona, K. de la Caba, *Carbohydr. Polym.* **2019**, *206*, 820.
[18] Q. Liu, Y. Wang, S. Sun, F. Tang, H. Chen, S. Chen, C. Zhao, L. Li, *Chemosphere* **2023**, *313*, 137367.
[19] M. Schaffner, P. A. Rühs, F. Coulter, S. Kilcher, A. R. Studart, *Sci. Adv.* **2017**, *3*, aao6804.
[20] H. Amiri, M. Aghbashlo, M. Sharma, J. Gaffey, L. Manning, S. M. Moosavi Basri, J. F. Kennedy, V. K. Gupta, M. Tabatabaei, *Nat. Food* **2022**, *3*, 822.
[21] Q. Tian, S. Liu, X. Sun, H. Sun, Z. Xue, T. Mu, *Carbohydr. Res.* **2015**, *408*, 107.
[22] J. M. F. Pavoni, C. L. Luchese, I. C. Tessaro, *Int. J. Biol. Macromol.* **2019**, *138*, 693.
[23] L. Zhang, M. Zhang, B. Adhikari, L. Zhang, *Food Hydrocoll.* **2023**, *139*, 108538.
[24] H. Lundberg, F. Tinnis, N. Selander, H. Adolfsson, *Chem. Soc. Rev.* **2014**, *43*, 2714.
[25] L. Hu, P. Zhang, X. Wang, X. Cheng, J. Qin, R. Tang, *Carbohydr. Polym.* **2017**, *178*, 166.
[26] S. Botelho da Silva, M. Krolicka, L. A. M. van den Broek, A. E. Frissen, C. G. Boeriu, *Carbohydr. Polym.* **2018**, *186*, 299.
[27] C. Niu, N. Zhang, C. Hu, C. Zhang, H. Zhang, Y. Xing, *Carbohydr. Polym.* **2021**, *258*, 117644.
[28] N. Zhang, H. Zhang, R. Li, Y. Xing, *Int. J. Biol. Macromol.* **2020**, *152*, 1146.
[29] K. Liu, W. Burlant, *J. Polym. Sci.* **1967**, *5*, 1407.
[30] A. Dobaj Štiglic, R. Kargl, M. Beaumont, C. Strauss, D. Makuc, D. Egger, J. Plavec, O. J. Rojas, K. Stana Kleinschek, T. Mohan, *ACS Biomater. Sci. Eng.* **2021**, *7*, 3618.
[31] G. M. Liao, C. C. Yang, C. C. Hu, Y. L. Pai, S. J. Lue, *J. Membr. Sci.* **2015**, *485*, 17.
[32] A. Zhang, Y. Han, Z. Zhou, *Food Hydrocoll.* **2023**, *135*, 108144.
[33] H. Charville, D. Jackson, G. Hodges, A. Whiting, *Chem. Commun.* **2010**, *46*, 1813.
[34] Y. Wang, L. Dong, R. Xiong, A. Hu, *J. Mater. Chem. C Mater.* **2013**, *1*, 7731.
[35] L. Zhuang, X. Zhi, B. Du, S. Yuan, *ACS Omega* **2020**, *5*, 1086.
[36] Y. Wang, S. Chen, Y. Yao, N. Wu, M. Xu, Z. Yin, Y. Zhao, Y. Tu, *Int. J. Biol. Macromol.* **2023**, *229*, 268.
[37] D. Nataraj, S. Sakkara, M. Meghwal, N. Reddy, *Int. J. Biol. Macromol.* **2018**, *120*, 1256.
[38] K. Okuyama, K. Noguchi, T. Miyazawa, T. Yui, K. Ogawa, *Macromolecules* **1997**, *30*, 5849.
[39] F. Feng, Y. Liu, K. Hu, *Carbohydr. Res.* **2004**, *339*, 2321.
[40] Y. Zhang, C. Xue, Y. Xue, R. Gao, X. Zhang, *Carbohydr. Res.* **2005**, *340*, 1914.
[41] E. Podgorbunskikh, T. Kuskov, D. Rychkov, O. Lomovskii, A. Bychkov, *Polymers (Basel)* **2022**, *14*, 4438.
[42] K. Okuyama, K. Noguchi, M. Kanenari, T. Egawa, K. Osawa, K. Ogawa, *Carbohydr. Polym.* **2000**, *41*, 237.
[43] D. Baskar, T. S. Sampath Kumar, *Carbohydr. Polym.* **2009**, *78*, 767.
[44] H. Wu, Y. Lei, J. Lu, R. Zhu, D. Xiao, C. Jiao, R. Xia, Z. Zhang, G. Shen, Y. Liu, S. Li, M. Li, *Food Hydrocoll.* **2019**, *97*, 105208.
[45] I. Zarandona, N. C. Minh, T. S. Trung, K. de la Caba, P. Guerrero, *Int. J. Biol. Macromol.* **2021**, *182*, 1331.
[46] L. C. Tomé, N. H. C. S. Silva, H. R. Soares, A. S. Coroadinha, P. Sadocco, I. M. Marrucho, C. S. R. Freire, *Green Chem.* **2015**, *17*, 4291.
[47] S. lin Yang, Z. H. Wu, W. Yang, M. B. Yang, *Polym. Test.* **2008**, *27*, 957.
[48] Q. Meng, M. C. Heuzey, P. J. Carreau, *Biomacromolecules* **2014**, *15*, 1216.
[49] K. Sakurai, T. Maegawa, T. Takahashi, *Polymer (Guildf)* **2000**, *41*, 7051.
[50] M. G. Abiad, O. H. Campanella, M. T. Carvajal, *Pharmaceutics* **2010**, *2*, 78.
[51] Y. Suzuki, T. Kano, T. Tomii, N. Tsuji, A. Matsumoto, *Polymers (Basel)* **2022**, *14*, 4876.
[52] N. G. Madian, N. Mohamed, *J. Mater. Res. Technol.* **2020**, *9*, 12970.
[53] I. Quijada-Garrido, V. Iglesias-González, J. M. Mazón-Arechederra, J. M. Barrales-Rienda, *Carbohydr. Polym.* **2007**, *68*, 173.
[54] M. C. Montoya-Ospina, H. Verhoogt, M. Ordner, X. Tan, T. A. Osswald, *Polym. Eng. Sci.* **2022**, *62*, 4203.
[55] C. M. Ninciuleanu, R. Ianchis, E. Alexandrescu, C. I. Mihaescu, C. Scomoroscenco, C. L. Nistor, S. Preda, C. Petcu, M. Teodorescu, *Materials* **2021**, *14*, 2305.
[56] Y. Campos, F. J. Sola, G. Fuentes, L. Quintanilla, A. Almirall, L. J. Cruz, J. C. Rodríguez-Cabello, Y. Tabata, *Polymers (Basel)* **2021**, *13*, 907.
[57] S. Niamlang, S. Thongchai, N. Pawananant, A. Sirivat, *Energy Proc.* **2013**, *34*, 697.
[58] S. Jiang, C. Qiao, R. Liu, Q. Liu, J. Xu, J. Yao, *Carbohydr. Polym.* **2023**, *312*, 120842.
[59] Z. Jiang, S. M. Easa, C. Hu, X. Zheng, *Constr. Build. Mater.* **2020**, *242*, 118185.
[60] G. Charon, J. Peixinho, L. Michely, A. Guinault, V. Langlois, *J. Appl. Polym. Sci.* **2022**, *139*, 53052.
[61] O. Y. Alothman, S. Awad, R. Siakeng, E. M. Khalaf, H. Fouad, N. M. Abd El-salam, F. Ahmed, M. Jawaid, *Polym. Eng. Sci.* **2023**, *63*, 1234.

[62] D. Aydemir, D. J. Gardner, *Polym. Compos.* **2020**, *41*, 3842.
[63] W. Zhang, T. Zhang, N. Jiang, T. Zhang, *J. Polym. Res.* **2020**, *27*, 163.
[64] M. K. Gupta, R. Singh, *Mater. Today Proc.* **2018**, *5*, 6109.
[65] E. Rodriguez, M. Larrañaga, I. Mondragón, A. Vázquez, *J. Appl. Polym. Sci.* **2006**, *100*, 3895.
[66] B. Brylka, M. Schemmann, J. Wood, T. Böhlke, *Polym. Test.* **2018**, *66*, 296.
[67] K. Aouachria, N. Belhaneche-Bensemra, V. Massardier-Nageotte, *J. Vinyl Addit. Technol.* **2011**, *17*, 156.
[68] S. Yoo, C. Holloman, D. Tomasko, K. Koelling, M. A. Pascall, *Packag. Technol. Sci.* **2014**, *27*, 169.
[69] J. Huang, Y. Zhong, L. Zhang, J. Cai, *Adv. Funct. Mater.* **2017**, *27*, 1701100.
[70] M. Li, D. Li, L. J. Wang, B. Adhikari, *Carbohydr. Polym.* **2015**, *117*, 957.
[71] L. Bisharat, A. Berardi, D. R. Perinelli, G. Bonacucina, L. Casettari, M. Cespi, H. S. AlKhatib, G. F. Palmieri, *Int. J. Biol. Macromol.* **2018**, *106*, 360.
[72] J. A. Sirviö, M. Visanko, J. Ukkola, H. Liimatainen, *Ind. Crops Prod.* **2018**, *122*, 513.
[73] K. Yang, K. Yazawa, K. Tsuchiya, K. Numata, J. Guan, *Biomacromolecules* **2019**, *20*, 2295.
[74] Y. Boussès, N. Brulat-Bouchard, P. O. Bouchard, H. Abouelleil, Y. Tillier, *Dent. Mater.* **2020**, *36*, 97.
[75] U. G. K. Wegst, H. Bai, E. Saiz, A. P. Tomsia, R. O. Ritchie, *Nat. Mater.* **2015**, *14*, 23.
[76] C. Guo, C. Li, H. V. Vu, P. Hanna, A. Lechtig, Y. Qiu, X. Mu, S. Ling, A. Nazarian, S. J. Lin, D. L. Kaplan, *Nat. Mater.* **2020**, *19*, 102.
[77] R. W. Korsmeyer, R. Gurny, E. Doelker, P. Buri, N. A. Peppas, *Int. J. Pharm.* **1983**, *15*, 25.
[78] N. T. N. Vo, L. Huang, H. Lemos, A. L. Mellor, K. Novakovic, *J. Appl. Polym. Sci.* **2021**, *138*, 50848.
[79] S. L. Reay, E. L. Jackson, A. M. Ferreira, C. M. U. Hilkens, K. Novakovic, *Mater. Adv.* **2022**, *3*, 7946.
[80] Y. Hong, H. Song, Y. Gong, Z. Mao, C. Gao, J. Shen, *Acta Biomater.* **2007**, *3*, 23.
[81] I. M. El-Sherbiny, H. D. C. Smyth, *J. Microencapsul.* **2010**, *27*, 657.
[82] Q. Zhang, Y. Jiang, Y. Zhang, Z. Ye, W. Tan, M. Lang, *Polym. Degrad. Stab.* **2013**, *98*, 209.
[83] A. Nowak, J. Żur-Pińska, A. Piński, G. Pacek, A. Mrozik, *Ecotoxicol. Environ. Saf.* **2021**, *221*, 112431.
[84] E. Kurzbaum, Y. Raizner, O. Cohen, R. Y. Suckeveriene, A. Kulikov, B. Hakimi, L. Iasur Kruh, R. Armon, Y. Farber, O. Menashe, *Water Res.* **2017**, *121*, 37.
[85] P. J. Allsop, Y. Chisti, M. Moo-Young, G. R. Sullivan, *Biotechnol. Bioeng.* **1993**, *41*, 57.
[86] P. Sahariah, G. I. Kontogianni, E. Scoulica, O. E. Sigurjonsson, M. Chatzinikolaidou, *Carbohydr. Polym.* **2023**, *312*, 120796.